Transport of Energetic Ions due to Microturbulence, Sawteeth, and Alfvén Eigenmodes

D. C. Pace[1], R. K. Fisher[2], M. García-Muñoz[3], W. W. Heidbrink[1], Z. Lin[1], G. R. McKee[4], M. Murakami[5], C. M. Muscatello[1], R. Nazikian[6], J. M. Park[5], C. C. Petty[2], T. L. Rhodes[7], M. A. Van Zeeland[2], R. E. Waltz[2], R. B. White[6], J. H. Yu[8], W. Zhang[1] and Y. B. Zhu[1]

[1] University of California-Irvine, Irvine, California 92697, USA
[2] General Atomics, P.O. Box 85608, San Diego, California 92186-5608
[3] Max-Planck Institut für Plasmaphysik, Garching D-85748, Germany
[4] University of Wisconsin-Madison, 1500 Engineering Dr., Madison, Wisconsin 53706, USA
[5] Oak Ridge National Laboratory, PO Box 2008, Oak Ridge, Tennessee 37831,USA
[6] Princeton Plasma Physics Laboratory, PO Box 451, Princeton, New Jersey 08543-0451, USA
[7] University of California-Los Angeles, PO Box 957099, Los Angeles, CA 90095-7099, USA
[8] University of California-San Diego, 9500 Gilman Dr., La Jolla, California 92093, USA

E-mail: pacedc@fusion.gat.com

Abstract. Utilizing an array of new diagnostics and simulation/modeling techniques, recent DIII-D experiments have elucidated a variety of energetic ion transport behaviors in the presence of instabilities ranging from large-scale sawteeth to fine spatial scale microturbulence. Important new insights include: microturbulence can contribute to the removal of alpha ash while having little effect on fusion alphas; sawteeth, such as those of the ITER baseline scenario, cause major redistribution of the energetic ion population; and high levels of transport induced by low-amplitude Alfvén eigenmodes are due to the integrated effect of a large number of simultaneous modes.

1. Introduction

Understanding and controlling the confinement of energetic ion populations in tokamaks is increasing in importance as we approach self-heated devices. In ITER, seemingly small reductions in fusion-α confinement can significantly reduce fusion power, and direct losses impacting the first-wall have the ability to cause damage [1, 2]. Collaborative work combining experimental and theoretical research is focused on the creation of accurate models for describing this resultant transport. Developing validated predictive

models for the nonlinear interaction of energetic particles with plasma instabilities is vital for extrapolation to ITER and future devices since adequate confinement of the 3.5 MeV fusion born alpha particles is required in order to maintain a burning plasma state. Further, once these particles have deposited their energy, the challenge is to remove this alpha ash before it contributes significant fuel dilution limiting the fusion rate at the maximum beta.

Recent DIII-D experiments employing a wide array of diagnostics have studied a variety of energetic ion transport processes. At the fine spatial scale of microturbulence it is shown that ion temperature gradient (ITG) and trapped electron mode (TEM) turbulence can contribute to the removal of alpha ash while having little to no effect on full energy fusion alpha particles [3, 4]. In the intermediate scale of Alfvénic instabilities [5, 6, 7] such as the toroidal Alfvén eigenmode (TAE) and the reversed shear Alfvén eigenmode (RSAE), it is found that high levels of transport are due to the integrated effect of a large number of simultaneous but low-amplitude modes [8, 9]. At the large scale, sawteeth cause redistribution of the energetic ion population that is measurable across the entire poloidal cross section [10].

2. Transport by Microturbulence

Energetic ions are better confined than thermal particles, in part, because the large orbits of energetic ions allow them to average over microturbulence such as the ITG and TEM modes. Experiments at DIII-D [3, 4] featuring neutral beam injection and MHD quiescent plasmas, however, indicate differences between the measured energetic ion confinement and the predictions of neoclassical theory. Figure 1 shows a comparison between the neoclassical and experimentally observed radial profiles of the fast ion D_α (FIDA) density, which is proportional to the energetic ion density. A synthetic diagnostic that simulates the expected FIDA signal based on measured and calculated plasma parameters, FIDASIM [12], is used to compare theory with experimental observations.

Panel (a) of Figure 1 is taken from a discharge featuring an injected neutral beam power of $P_{inj} = 3.1$ MW and in which the ratio of thermal ion temperature to energetic ion energy, T_i/E, is everywhere below 0.11. Due to the thermalization process and the physics of neutral beam injection, there are ions of many energies simultaneously present in the plasma. Ranges for the ratio of T_i/E are provided using the peak ion temperature and a range of injected energies as a standardization representing the largest possibly encountered value in the experiment. In Figure 1, the theoretical profile (red $\diamond$ trace) is largely similar to the experimentally measured profile (black $\times$ trace). This agreement contrasts with the situation present in panel (b), where $P_{inj} = 7.2$ MW and T_i/E increases to a maximum value of 0.38. Panel (b) indicates that the experimentally measured profiles are considerably flatter than the expected profile. The vertical range is the same for each panel, illustrating that the expected and measured energetic ion densities have increased with increasing neutral beam injection power.

Recent theoretical and simulation work [13, 14, 15] shows that energetic ions of

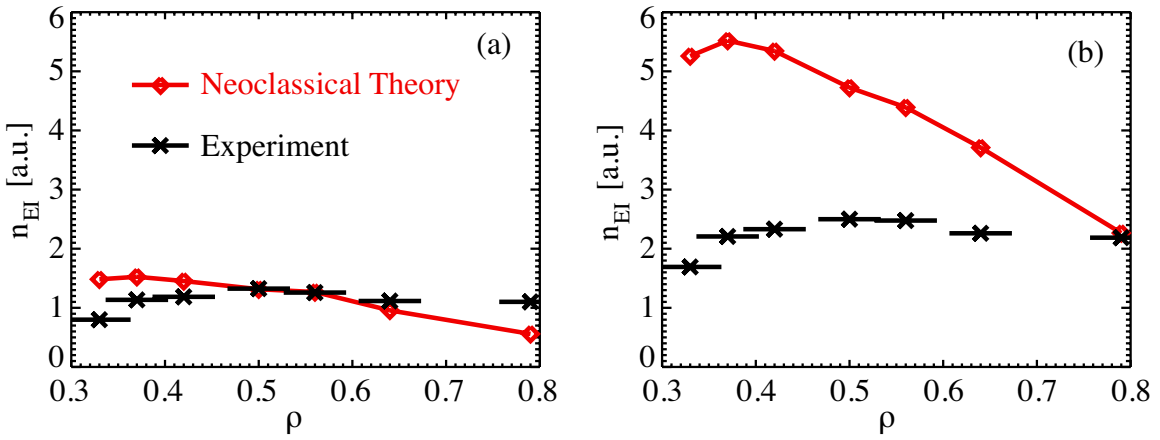

Figure 1. Radial profile (ρ = normalized square root of the toroidal magnetic flux) of proportional energetic ion density (FIDA density) as calculated based on classical, collision-dominated theory (red $\diamond$ trace) and from the FIDA simulation based on experimental measurements (black $\times$ trace). (a) Discharge 133981 with $P_{inj} = 3.1$ MW and FIDA data averaged over $2000 \leq t \leq 3000$ ms encompassing the range $0.02 \leq T_i/E \leq 0.11$. (b) Discharge 134426 with $P_{inj} = 7.2$ MW and FIDA data averaged over $2000 \leq t \leq 3000$ ms encompassing the range $0.13 \leq T_i/E \leq 0.38$.

beam energy in DIII-D are susceptible to microturbulence-induced transport. The transport enhancement due to microturbulence for beam ions is theoretically expected to scale as T_i/E. Based on this collection of theory and simulation results, an experiment was designed to maximize the value of T_i/E by reducing the injection energy of the DIII-D neutral beams.

Figure 2 displays FIDA spectra for a full beam energy discharge (left column) and for the reduced beam energy discharge (right column). Spectral radiance, as shown in this context, is a proxy for the energetic ion density. Values of spectral radiance that fall below theoretical expectations indicate that the energetic ion density is less than expected from classical theory. In both discharges, data is analyzed after the plasma current flattop but before the onset of sawteeth. The full energy discharge, 138385, injects four neutral beams all near 81 keV. The reduced energy discharge, 138392, injects five beam sources all near 58 keV. The spectral radiance is plotted as a function of perpendicular ion energy E_λ [16] and wavelength. Calibration uncertainty due to diagnostic window coatings developing over time is incorporated in the figure by plotting a secondary experimental trace featuring a 25% reduction in amplitude. The region of largest difference between theory and experiment occurs for $E_\lambda = 20 - 40$ keV, indicating that the effect is more pronounced for ions of lower perpendicular energy, which also feature smaller gyroradii.

This transport effect is modeled using TGYRO/TGLF [17, 18] to investigate the theoretically expected trend of increased energetic ion transport for larger values of T_i/E. Measured plasma profiles from the reduced neutral beam injection energy discharge, 138392, are provided as inputs to TGYRO/TGLF. The trace level energetic ion population is described by a Maxwellian with effective temperature $E_{\rm EI}$ varied in

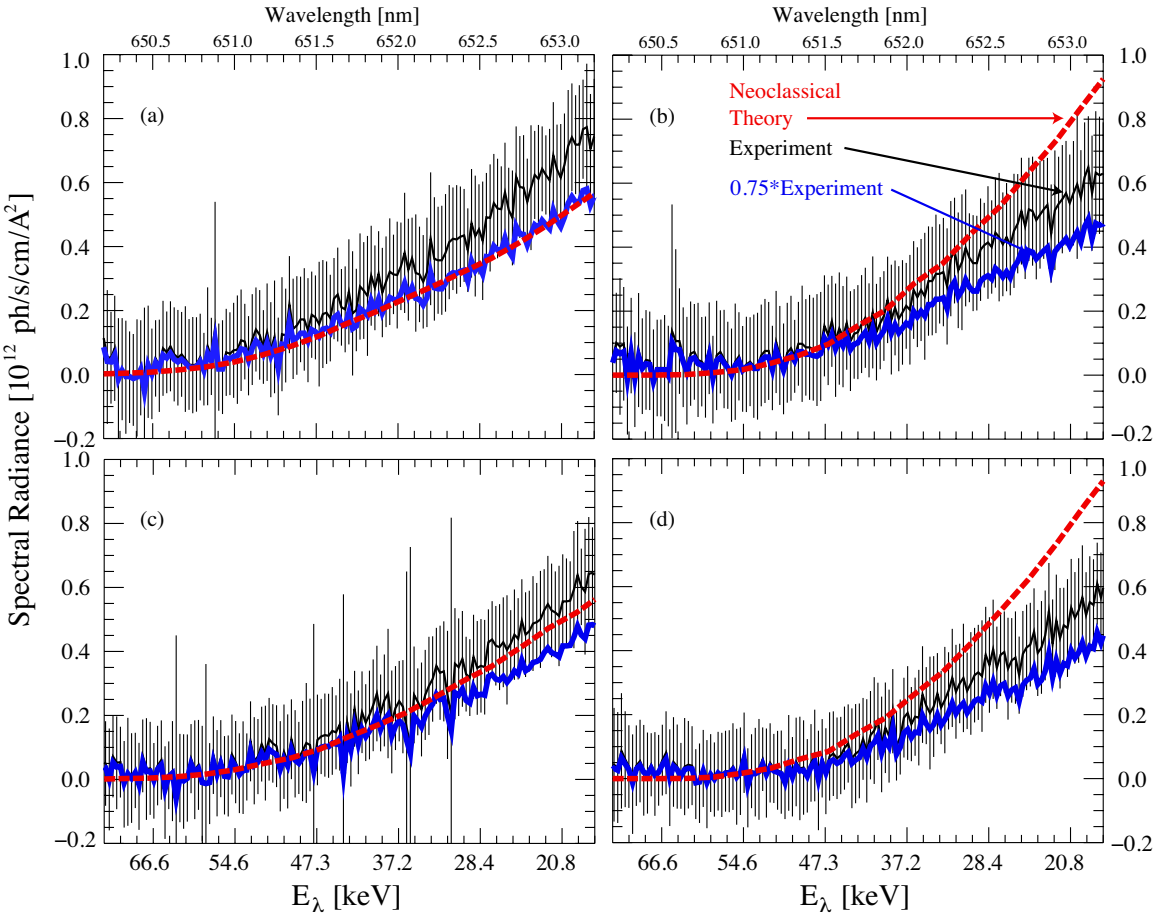

Figure 2. Comparison between measured FIDA spectra (black traces) and simulated spectra (red traces, using FIDASIM v2). The blue traces represent a 25% reduction in the experimental values that accounts for the largest possible change due to calibration uncertainty. Left Column: shot 138385, $E_{\text{inj}} = 81$ keV. Right Column: shot 138392, $E_{\text{inj}} = 58$ keV. (a) $\rho \approx 0.17$, (b) $\rho \approx 0.19$, (c) $\rho \approx 0.32$, (d) $\rho \approx 0.34$.

proportion to the fixed electron temperature ($T_e \approx T_i$). It is evident that as the energy of ions decreases, the turbulent particle diffusivity approaches that of the thermal ions. Furthermore, the effect increases towards the core, which supports the previously mentioned observations of reduced energetic ion density in the DIII-D studies. Future work will incorporate a slowing down distribution that better represents ions from neutral beam injection. Existing work comparing these different distributions finds that trends as a function of ion energy are consistent in both descriptions [19].

3. Transport by Sawtooth Oscillations

Redistribution of the energetic ion population due to a sawtooth crashes was originally observed in JET [20] and TFTR [21]. Recently, the effect has been quantified by both collective Thomson scattering [22] and FIDA [10] diagnostics on TEXTOR and DIII-D, respectively. Energetic ion density in the core is observed to decrease by nearly 50% in

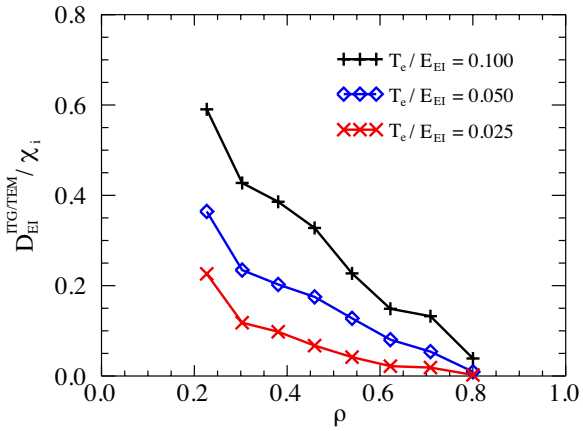

Figure 3. Radial profile of the energetic particle diffusivity due to ITG and TEM turbulence, $D_{EI}^{\mathrm{ITG/TEM}}$, normalized to the thermal ion energy diffusivity, χ_i, as calculated using TGYRO-TGLF for shot 138392. The energy of the energetic ion population is described by an equivalent Maxwellian temperature that is varied in proportion to the measured electron temperature.

Table 1. Properties of Gaussian shapes describing the FIDA density profiles before and after a sawtooth crash.

Property	Before	After
Center Position [m]	1.65	1.64
Full Width at Half-Maximum [m]	0.37	0.61
Fit χ^2	2.20	0.60

these cases. The DIII-D work incorporates a FIDA Imaging (FIDAI) system, which is a two-dimensional imaging diagnostic that provides observations across the entire poloidal cross-section. By removing the dependence of the beam injected neutral density profile, the FIDAI signal from this diagnostic (see Figure 6 of [10]) can be presented as a FIDA density that represents the energetic ion density.

Figure 4 displays representative (a) electron density and (b) energetic ion density profiles for time periods before (black traces) a sawtooth crash and after (blue traces) in DIII-D discharge 141195. Time averaging is performed over 20 ms periods preceding and following a crash evident in data from an electron cyclotron emission diagnostic. The two-dimensional FIDAI data in 4(b) is averaged over an approximately 5 cm tall region centered on the peak signal, which is on the midplane.

The electron density profiles in 4(a) are shown because that parameter most directly influences the injected neutral density profiles. The modest change observed in electron density cannot account for the large change in FIDA density. In order to quantify the redistribution of energetic ions due to the sawtooth crash, the FIDA density profiles are described by Gaussian fits that are plotted as red traces in Figure 4(b). Properties of these fits are given in Table 1.

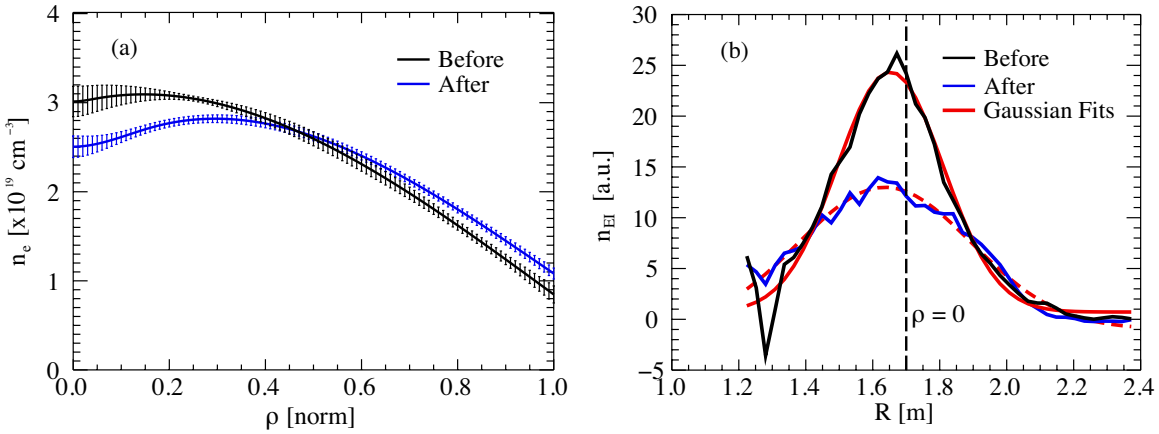

Figure 4. Discharge 141195: (a) Electron density representative of a time period before (black trace) and after (blue trace) a sawtooth crash. (b) FIDA density, n_{EI}, corresponding to the time periods before and after a sawtooth crash. Gaussian fits to these profiles are shown in red (dashed line for the after-crash fit).

From the results shown in Table 1 it is clear that the sawtooth crash widens the energetic ion profile without causing a shift. The after-crash profile is 65% wider than the before-crash profile according to the full width at half-maximum. The addition of a tangentially viewing FIDA diagnostic [23] at DIII-D allows for separately studying sawtooth effects according to whether the ions are on trapped or passing orbits. Transport dependencies related to sawtooth type and ion distribution will be compared with theoretical predictions in a separate work [24].

4. Transport by Alfvén Eigenmodes

In reversed shear plasmas with many small amplitude ($\delta B/B \approx 2 \times 10^{-4}$) toroidal and reversed-shear Alfvén eigenmodes, the central energetic ion profile flattens. Initial calculations failed to reproduce the experimental results [25, 26] but new calculations that utilize hundreds of harmonics and include the inductive electric field predict diffusive energetic ion transport at the observed level [8, 9].

ORBIT [27] calculations are performed using beam ion depositions from the NUBEAM [28, 29] module of TRANSP [30] based on measured plasma profiles. It is vital that energetic ion transport models account for the time dependence of the beam ion distribution, as seen in the flattening of the profiles in Figure 5. Energetic (beam) ion density profiles are plotted for the initial neutral beam injection time (0 ms) and after a slowing-down time (66 ms) at which the distribution has reached steady state. This steady state distribution produces a theoretical profile that approaches the two independent experimental observations from the FIDA density (filled red triangles) and MSE-EFIT analysis (dotted red trace). The MSE-EFIT profile is determined from the energetic ion pressure contribution using EFIT [31] equilibria constrained by motional Stark effect measurements of the magnetic field pitch.

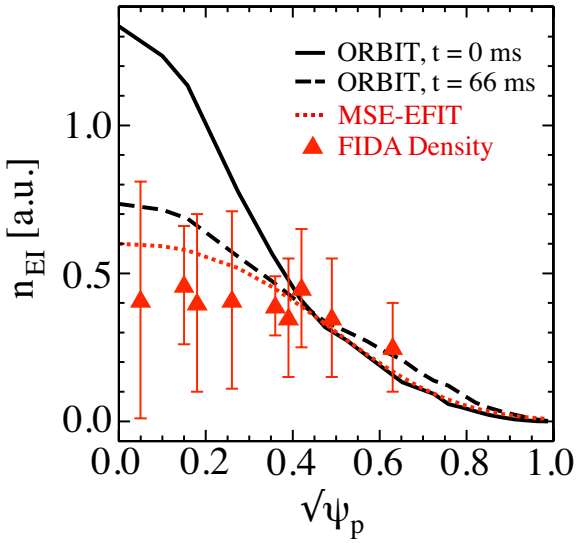

Figure 5. Energetic ion density as a function of the normalized square-root of the poloidal flux $\sqrt{\psi_p}$, for DIII-D discharge 122117. Experimental results are shown for both the FIDA density (filled red triangles), and from a calculation of the energetic ion pressure based on MSE-EFIT results [25] (dotted red trace). Theoretical results from ORBIT include slowing down processes. These are calculated for the initial neutral beam injection defined as $t = 0$ ms (solid black trace) and after a slowing-down time at which $t = 66$ ms (dashed black trace). This data is compiled in [9].

Modeling and simulations such as those leading to Figure 5 serve to improve our understanding of Alfvén eigenmode-induced transport in the core, but it remains to link these effects with losses observed at the vessel walls [32, 33]. A newly commissioned fast ion loss detector (FILD) [34] at DIII-D observes fluctuations in ion flux that are coherent at frequencies in the TAE/RSAE range ($60-100$ kHz). The FILD consists of a scintillator surface that emits light due to energetic ion impacts. This light is imaged by a camera for a two-dimensional signal that represents the energy and pitch angle of the ions. A photomultiplier tube (PMT) is also focused on the scintillator surface in order to measure fast (1 MHz) signals. Figure 6(a) shows an autopower spectrum from the FILD PMT signal averaged over a time period of Alfvén eigenmode activity ($510-540$ ms) and a later time during which most of this activity has subsided ($710-740$ ms). Peaks in the spectrum corresponding to Alfvén eigenmode activity are observed during the earlier time within the frequency range $60-90$ kHz. The relevant loss activity has disappeared by the later time window. The FILD camera data indicates that these losses are ions with an energy of $E \approx 80$ keV and pitch of $v_{\|}/v \approx 0.68$. Using this data and the known position of the FILD aperture, the orbit representing a typical lost ion is shown in Figure 6(b). As expected, this orbit is capable of originating from well within the last closed flux surface in a region where Alfvén eigenmodes are known to exist [35]. Efforts are underway to incorporate loss calculations into the modeling performed by ORBIT to provide a more complete treatment of energetic ion transport.

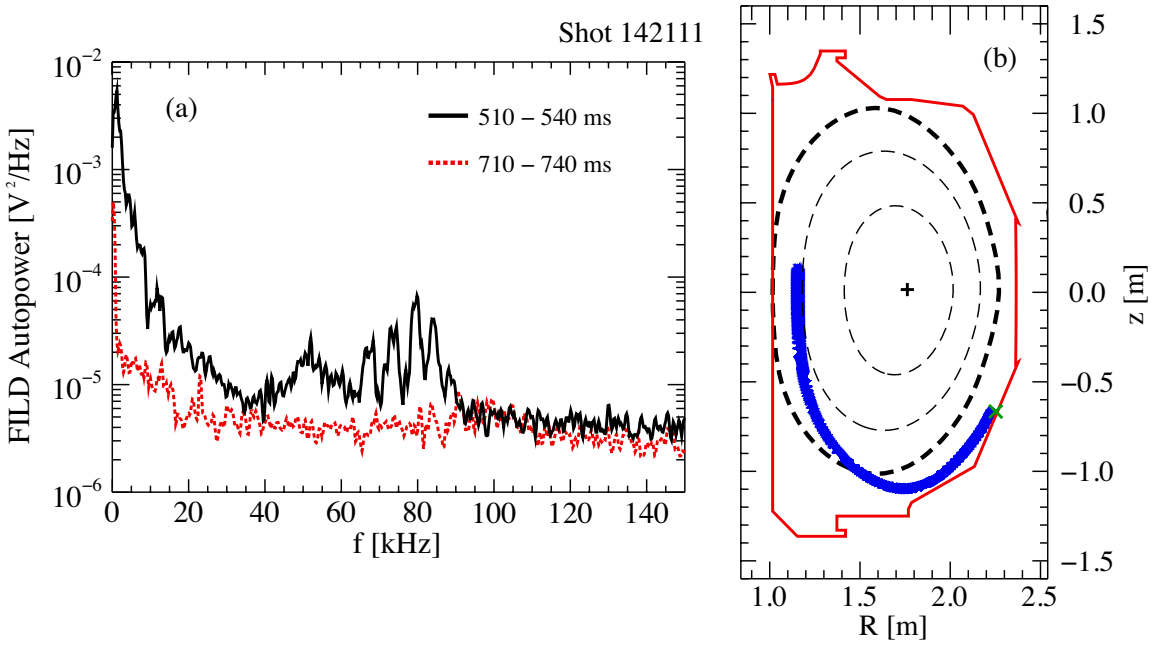

Figure 6. Energetic ion loss measures from DIII-D discharge 142111. (a) Autopower spectrum from the FILD PMT signal averaged over $510 \leq t \leq 540$ ms (solid black) and $710 \leq t \leq 740$ ms (dotted red). (b) Trajectory of a typical loss orbit (solid blue trace) based on FILD camera data at $t = 525$ ms. The full orbit trajectory has been averaged to reduce the number of points plotted. Ion orbit properties are: $E_o = 80$ keV, $v_\parallel/v = 0.676$ (47.5^o), FILD aperture position $[R, z] = [2.252, -0.666]$ m (indicated by the green $\times$).

5. Conclusion

A wide array of energetic ion transport studies are performed at DIII-D. These experiments observe transport effects due to microturbulence, sawtooth oscillations, and Alfvén eigenmodes. The presence of long wavelength turbulent modes such as the ITG and TEM contributes to the radial diffusion of energetic ions. This turbulent transport is predicted to increase with plasma temperature, but also as the energetic ion population thermalizes. The consequence for ITER operation is that fusion alphas ($T_i/E << 1$) should experience little to no transport enhancement and that alpha ash ($T_i/E \approx 1$) will be affected and therefore more easily extracted from the plasma. Improvements to diagnostic techniques will allow for experimental feedback to the growing collection of theory work concerning fusion alpha and alpha ash transport [13, 19, 36] in the ITER regime.

Continuing investigation of this turbulent transport will require improvements in both the ability to measure the effect in experiments and the ability to model it in simulations. In large-scale simulations that are the first of their kind, the gyrokinetic toroidal code (GTC) [37] is used to simulate both the microturbulence and the energetic ion response taking experimentally measured plasma profiles as input parameters. This aspect of the project uses measured plasma profiles from relevant DIII-D discharges.

Values for the energetic ion diffusivity obtained from GTC simulations are provided to TRANSP, which then calculates the resulting energetic ion profiles for comparison with experimental measurements.

During sawtooth crashes, a significant reduction in the core energetic ion density is observed. A two-dimensional FIDAI system measures energetic ion redistribution after the crash and indicates that profiles widen by 65%. In ITER, such a large redistribution of fusion alphas in the core implies a dramatic performance reduction. Present work in this area involves quantifying the difference in sawtooth response between the passing and trapped energetic ion populations [38]. Given the potentially complex phase space dependency of this interaction it remains a challenge to develop an accurate model that can predict the effect of sawtooth crashes on reactor performance.

Alfvén eigenmodes such as TAEs contribute to energetic ion transport even in cases where the mode amplitude is very small, $\delta B/B \approx 2 \times 10^{-4}$. Accurate treatment of the slowing-down distribution of the ions is vital to reproducing the measured effects on transport. Ion losses due to Alfvén eigenmodes are observed reaching detectors along the walls of multiple tokamaks [32, 33, 39]. A new procedure for modeling these coherent losses is being developed using the results of ORBIT, which simulates interactions between Alfvén waves and ions. ORBIT can follow ions to the separatrix, and a full-orbit calculation code tracks these particles to determine whether they strike the wall. Time dependence is taken into account and allows for modeling of losses due directly to the presence of a given mode.

Acknowledgments

This work was supported by the US Department of Energy under SC-G903402, DE-FC02-04ER54698, DE-FG02-89ER53296, DE-FG02-08ER54999, DE-AC05-00OR22725, DE-AC02-09CH11466, DE-FG03-08ER54984, and SciDAC GSEP.

References

[1] ITER Physics Expert Group on Energetic Particles and Heating and Current Drive and ITER Physics Basis Editors. 1999 *Nucl. Fusion* **39** 2471
[2] Fasoli A, et al. 2007 *Nucl. Fusion* **47** S264
[3] Heidbrink W W, Park J M, Murakami M, Petty C C, Holcomb C, and Van Zeeland M A. 2009 *Phys. Rev. Lett.* **103** 175001
[4] Heidbrink W W, Murakami M, Park J M, Petty C C, Van Zeeland M A, Yu J H and McKee G R. 2009 *Plasma Phys. Control. Fusion* **51** 125001
[5] Cheng C Z, Chen L and Chance M S. 1985 *Ann. Physics* **161** 21
[6] Cheng C Z and Chance M S. 1986 *Phys. Fluids* **29** 3695
[7] Sharapov S E, et al. 2002 *Phys. Plasmas* **9** 2027
[8] White R B, Gorelenkov N, Heidbrink W W and Van Zeeland M A. 2010 *Plasma Phys. Cont. Fusion* **52** 045012
[9] White R B, Gorelenkov N, Heidbrink W W and Van Zeeland M A. 2010 *Phys. Plasmas* **17** 056107
[10] Van Zeeland M A, et al. 2010 *Nucl. Fusion* **50** 084002

[11] Heidbrink W W , Burrell K H, Luo Y, Pablant N A and Ruskov E. 2004 *Plasma Phys. Control. Fusion* **46** 1855
[12] Heidbrink W W, Liu D, Luo Y, Ruskov E and Geiger B. 2010 *submitted to Communications in Computational Physics*
[13] Estrada-Mila C, Candy J and Waltz R E. 2006 *Phys. Plasmas* **13** 112303
[14] Zhang W, Lin Z and Chen L. 2008 *Phys. Rev. Lett.* **101** 095001
[15] Hauff T, Pueschel M J, Dannert T and Jenko F. 2009 *Phys. Rev. Lett.* **102** 075004
[16] Heidbrink W W, Luo Y, Burrell K H, Harvey R W, Pinsker R I and Ruskov E. 2007 *Plasma Phys. Control. Fusion* **49** 1457
[17] Candy J, Holland C, Waltz R E, Fahey M R and Belli E. 2009 *Phys. Plasmas* **16** 060704
[18] Kinsey J E, Staebler G M and Waltz R E. 2008 *Phys. Plasmas* **15** 055908
[19] Angioni C and Peeters A G. 2008 *Phys. Plasmas* **15** 052307
[20] Anderson D, Batistoni P, Lisak M and Wising F. 1993 *Plasma Phys. Control. Fusion* **35** 733
[21] Fisher R K, et al. 1995 *Phys. Rev. Lett.* **75** 846
[22] Nielsen S K, et al. 2010 *Plasma Phys. Control. Fusion* **52** 092001
[23] Muscatello C M, Heidbrink W W, Taussig D and Burrell K H. "Extended Fast-Ion D-Alpha (FIDA) Diagnostic on DIII-D" 2010 *Rev. Sci. Instrum.* In press
[24] Muscatello C M, ...
[25] Heidbrink W W, et al. 2007 *Phys. Rev. Lett.* **99** 245002
[26] Heidbrink W W, et al. 2008 *Nucl. Fusion* **48** 084001
[27] White R B and Chance M S. 1984 *Phys. Fluids* **27** 2455
[28] Goldston R J, McCune D C, Towner H H, Davis S L, Hawryluk R J and Schmidt G L. 1981 *J. Comp. Physics* **43** 61
[29] Pankin A, McCune D, Andre R, Bateman G and Kritz A. 2004 *Comp. Physics Comm.* **159** 157
[30] See *http://w3.pppl.gov/transp*, the official home page of TRANSP, for information regarding the models and methods employed and usage documentation.
[31] Lao L L, St. John H, Stambaugh R D, Kellman A G and Pfeiffer W. 1985 *Nucl. Fusion* **25** 1611
[32] Duong H H, Heidbrink W W, Strait E J, Petrie T W, Lee R, Moyer R A and Watkins J G. 1993 *Nucl. Fusion* **33**, 749
[33] García-Muñoz M, et al. 2008 *Phys. Rev. Lett.* **100**, 055005
[34] Fisher R K, Pace D C, García-Muñoz, Heidbrink W W, Muscatello C M, Van Zeeland M A and Zhu Y B. "Scintillator-Based Diagnostic for Fast Ion Loss Measurements on DIII-D" 2010 *Rev. Sci. Instrum.* In press
[35] Van Zeeland M A, et al. 2006 *Phys. Rev. Lett.* **97** 135001
[36] Estrada-Mila C, Candy J, and Waltz R E. 2005 *Phys. Plasmas* **12** 022305
[37] Lin Z, Hahm T S, Lee W W, Tang W M and White R B. 1998 *Science* **281** 1835
[38] Muscatello C M, Heidbrink W W, Lazarus E A, Van Zeeland M A and Yu J H. 2009 "Fast Ion Transport due to the Sawtooth Collapse in the DIII-D Tokamak," P36 *11^{th} IAEA Technical Meeting Energetic Particles in Magnetic Confinement Systems*, Kyiv, Ukraine http://www.kinr.kiev.ua/TCM/index.html
[39] Darrow D S, Fredrickson E D, Gorelenkov N N, Roquemore A L and Shinohara K. 2008 *Nucl. Fusion* **48** 084004